

Olfactory ensheathing cells from the nasal mucosa and olfactory bulb have distinct membrane properties

Running title: Membrane currents in olfactory ensheathing cells

Authors: Katie E. Smith¹, Katherine Whitcroft^{1,2}, Stuart Law³, Peter Andrews^{1,2}, David Choi³, and Daniel J. Jagger^{1#}

Affiliations: ¹UCL Ear Institute, University College London, London UK; ²Royal National Throat Nose & Ear Hospital, London UK; ³Institute of Neurology, University College London, London UK.

Correspondence: #Correspondence should be addressed to Daniel J. Jagger, UCL Ear Institute, University College London, 332 Gray's Inn Road, London, WC1X 8EE, United Kingdom. Email: d.jagger@ucl.ac.uk.

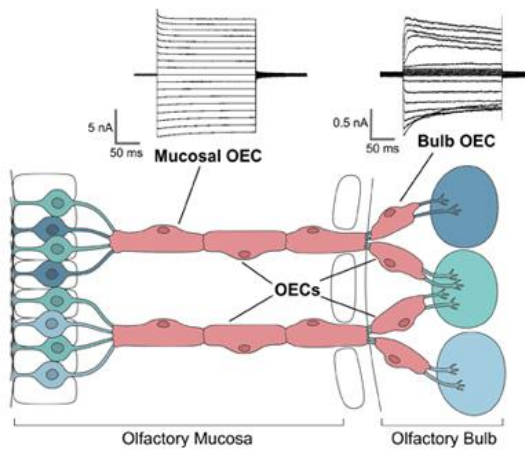
Acknowledgements: This study was supported by an Action on Hearing Loss/Dunhill Medical Trust Pauline Ashley Fellowship to KES (PA24), grants from the Biotechnology and Biological Sciences Research Council to DJJ (BB/M019322/1 and BB/R000549/1), and a grant from the Wellcome Trust to DC (200134/Z/15/Z). The work was carried out in part at the UCL/UCLH Biomedical Research Centre.

Keywords: Patch clamp, electrophysiology, ion channels, glia, olfaction, RRID:AB_141607, RRID:AB_162543, RRID:AB_664696, RRID:AB_2040120, RRID:AB_2313773, RRID:AB_2340962, RRID:AB_2534117, RRID:AB_2535739, RRID:AB_2535775, RRID:AB_10013383.

Word count (section and total): Abstract: 243; Significance Statement: 97; Introduction: 842; Materials and Methods: 1380; Results: 1312; Discussion: 1587; Total: 8449.

Figures: 7 + 1 Graphical Abstract

Graphical Abstract Text



Olfactory ensheathing cells (OECs) are specialized glia, which wrap the axons of olfactory neurons that mediate the sense of smell. Their physiological roles during olfaction are largely unknown. Our electrophysiological characterization suggests that peripheral and central OECs are functionally distinct. Peripheral OECs have large weak inward rectifier currents, whereas central OECs have smaller strong inward rectifier currents and strong outward rectifier currents. These distinct sets of membrane properties may point to regional specializations *in vivo*.

Abstract

Transplantation of Olfactory Ensheathing Cells (OECs) is a potential therapy for the regeneration of damaged neurons. While they maintain tissue homeostasis in the olfactory mucosa (OM) and olfactory bulb (OB), their regenerative properties also support the normal sense of smell by enabling continual turnover and axonal regrowth of olfactory sensory neurons (OSNs). However, the molecular physiology of OECs is not fully understood, especially that of OECs from the mucosa. Here, we carried out whole-cell patch clamp recordings from individual OECs cultured from the OM and OB of the adult rat, and from the human OM. A subset of OECs from the rat OM cultured 1-3 days *in vitro* (DIV) had large weakly rectifying K⁺ currents, which were sensitive to Ba²⁺ and desipramine, blockers of Kir4-family channels. Kir4.1 immunofluorescence was detectable in cultured OM cells co-labelled for the OEC marker S100, and in S100-labelled cells found adjacent to OSN axons in mucosal sections. OECs cultured from rat OB had distinct properties though, displaying strongly rectifying inward currents at hyperpolarized membrane potentials and strongly rectifying outward currents at depolarized potentials. Kir4.1 immunofluorescence was not evident in OECs adjacent to axons of OSNs in the OB. A subset of human OECs cultured from the OM of adults had membrane properties comparable to those of the rat OM, i.e. dominated by Ba²⁺-sensitive weak inwardly rectifying currents. The membrane properties of peripheral OECs are different to those in central OECs, suggesting they may play distinct roles during olfaction.

Significance Statement

Harnessing the regenerative abilities of olfactory glia is widely proposed as a strategy to re-grow nerve cells in the damaged central nervous system. Nasal mucosa biopsies represent a relatively non-invasive source of these cells for patient therapies. In this study, we determined the necessary experimental conditions required to characterize the membrane properties of the peripheral glia. Surprisingly, we found that peripheral olfactory glia have different properties to those in the brain.

Additionally, our study identified a candidate membrane protein that may help identify and purify these cells in future studies, and to refine current cell transplantation approaches.

Introduction

Olfactory ensheathing cells (OECs) are specialized glia that bridge the boundary between the peripheral and central tissues mediating the sense of smell. The physiology of OECs remains poorly understood, but their inherent abilities appear to support the continual renewal of olfactory sensory neurons (OSNs) under normal conditions (Gomez et al., 2018). Around five to six million OSNs reside within the nasal sensory epithelium (de Castro, 2009; Jafek, 1983). Accompanied by OECs, their axons fasciculate to form the first cranial nerve that projects to the olfactory bulb (OB). These axons, which are thin and unmyelinated (Garcia-Gonzalez, Murcia-Belmonte, Clemente, & De Castro, 2013), enter the OB within the outer nerve layer (ONL), where they continue to be wrapped by OECs. The axons then coalesce into large glomeruli where they relay with mitral and tufted cells. The axons of these projection neurons form the lateral olfactory tract (LOT) that leads to the olfactory cortex where information is processed. The majority of axons within the LOT are myelinated, a process mediated by oligodendrocytes (Garcia-Gonzalez et al., 2013).

The lifespan of OSNs is relatively short, around 30 days in young mammals (Brann & Firestein, 2014), and so there is a need for continual neurogenesis in order to maintain a normal sense of smell. Harnessing the unusual neuro-regenerative abilities of the olfactory system continues to be promoted as a therapeutic approach to the reversal of spinal cord injury and certain demyelinating conditions (Assinck, Duncan, Hilton, Plemel, & Tetzlaff, 2017; Ekberg & St John, 2014; Gladwin & Choi, 2015; Gomez et al., 2018; Yao et al., 2018). The olfactory mucosa (OM) represents a particularly attractive target for sourcing OECs for clinical transplantation, as it permits relatively non-invasive endoscopic harvesting from affected patients, healthy volunteers, or cadaveric specimens (Andrews, Poirrier, Lund, & Choi, 2016; Choi & Gladwin, 2015). In addition, several lines of evidence suggest OECs derived from the OM may be especially beneficial for transplantation therapies (Yao et al., 2018). The physiological functions of peripheral OECs remain poorly understood at a cellular and molecular level (Chen, Kachramanoglou, Li, Andrews, & Choi,

2014; Gomez et al., 2018), and so it is currently unclear why this subtype of OECs could more successfully encourage neuronal regeneration. Much of our current understanding of neuro-glia interactions comes from structural, molecular and functional studies of rodent OECs, from either the OM or OB (Guerout et al., 2010; Hayat, Wigley, & Robbins, 2003; Higashi et al., 2001; Piantanida et al., 2019; Rash et al., 2005; Rela, Bordey, & Greer, 2010; Rela, Piantanida, Bordey, & Greer, 2015; Rieger, Deitmer, & Lohr, 2007). Studies of excised human OM tissues have also helped identify common markers *in vivo* (Choi, Law, Raisman, & Li, 2008; Liu et al., 2010; Oprych, Cotfas, & Choi, 2017).

There is evidence of morphological, genetic, and functional heterogeneity between sub-populations of OECs (Gomez et al., 2018). OECs from the OB segregate into distinct phenotypic populations when maintained *in vitro* (Hayat et al., 2003). Some are spindle-shaped and Schwann cell-like, whereas others maintain a flattened astrocyte-like morphology, and these cell types display differences in their expression of glial markers (Honore et al., 2012). OECs within the OB and OM have distinct gene expression profiles (Guerout et al., 2010), but it is currently unclear whether these genetically and spatially separate populations mediate common physiological mechanisms that ensure normal homeostasis and continual neuronal turnover. Previous studies in acute slices of the OB from juvenile mice have described a variable contribution of certain types of membrane channels to shaping the electrical responses of OECs (Piantanida et al., 2019; Rela et al., 2010; Rela et al., 2015). Following the loss of gap-junctional coupling, these OECs display heterogeneous membrane currents, with variable contributions from hyperpolarization-activated inward rectifier K⁺ currents and depolarization-activated outward rectifier K⁺ currents. However, to date the molecular identities of the ion channel subtypes underlying these responses in central OECs remain undetermined. In addition, there is a lack of information available on the membrane properties of peripheral OECs.

In this study, we have determined the membrane properties of human OECs, harvested from patient biopsies of the nasal mucosa. In order to do this, we first employed a rat model to determine the culture procedures and recording conditions required for physiological characterization of biopsied cells *in vitro*. We employed whole-cell patch clamp to investigate the membrane properties of OECs cultured from the OM of adult rats, and surprisingly, found them to be distinct to those cultured from the rat OB. There was a strong resemblance, though, between the properties of rat OM OECs and of those harvested by endoscopic biopsy from the OM of humans. Weak rectifier currents dominated the electrical responses in OECs from the OM of both rats and humans, and consistent with these observations, there was expression of weak rectifier K⁺ channel subunits by OECs within lamina propria of the rat OM, and in cultured human OECs. The data provide the first description of the membrane properties of human peripheral OECs, and highlight region-specific differences that may help explain the physiological roles of these enigmatic glial cells.

Materials and Methods

Animals. Twelve-week old Sprague Dawley rats (purchased from Charles River or Harlan) were maintained in groups under a 12-hour light–dark cycle, and were given food and water ad libitum. Rats were killed by CO₂ inhalation followed by cervical dislocation. Tissues were used without regard to the sex of the animal. All animal work was in accordance with the UCL Animal Welfare and Ethical Review Body, and conformed to United Kingdom legislation outlined in the Animals (Scientific Procedures) Act 1986. A total of 10 rats were used in this study.

Human OEC donors. Adult patients undergoing functional septorhinoplasty under the care of PA were recruited. The surgical procedures for harvesting patient specimens largely followed those outlined elsewhere (Andrews et al., 2016; Kachramanoglou, Law, Andrews, Li, & Choi, 2013). All procedures were performed under United Kingdom National Health Service Research Ethics Committee approval (14/SC/1180) and patient informed consent. The patients' medical history was documented including age, sex, presenting complaint, past medical and surgical history, drug history including recent use of topical and/or oral steroids, allergies, and smoking status. Birhinal olfactory function was assessed using “Sniffin’ Sticks”, a validated psychophysical tool which separately tests odor threshold, discrimination and identification (Hummel, Kobal, Gudziol, & Mackay-Sim, 2007; Neumann et al., 2012). Detailed testing procedures are outlined elsewhere (Whitcroft, Cuevas, Haehner, & Hummel, 2017). Normosmia was assumed where composite threshold, discrimination and identification (TDI) score was ≥ 30.3 (Hummel et al., 2007). Patients with neurological, psychiatric or other conditions known to affect olfaction were excluded, as were those under 18 or over 70 years of age. Samples from three participants were obtained (male:female = 2:1; mean age 21 years, range 18-29). Two of the participants were normosmic according to composite TDI score. One participant scored within the high hyposmic range (TDI 27.75), though this was associated with significant nasal obstruction at the time of testing, and normalized at three months post-operatively.

Surgical procedure for human olfactory biopsies: Biopsies were harvested endoscopically during functional septorhinoplasty. A detailed description of the technique is outlined elsewhere (Kachramanoglou et al., 2013). In brief, full thickness biopsies were obtained (including bone, so ensuring integrity of the lamina propria) from the middle third of the superior turbinate. The nasal mucosa was prepared either with topical lignocaine with phenylephrine (lignocaine hydrochloride 5% and phenylephrine hydrochloride 0.5%) or Moffett's solution (2 mL 6% cocaine, 1 mL 1:1000 epinephrine, 2 mL 8% sodium bicarbonate solution), and the procedure performed under general anesthetic. Further vasoconstriction was obtained as required through use of topical epinephrine (1:10,000) soaked neuro patties. Once obtained, the specimen was immediately placed into ice-cold culture medium (DMEM/F-12 + GlutaMax, 10% fetal bovine serum (FBS), 1% penicillin-streptomycin, 1% insulin-transferrin-selenium) and transferred to the laboratory.

Rat and human OEC cultures. The olfactory tissue from two rats was used for each culture. For rat or human mucosal OEC cultures, mucosa were first washed in Hanks balanced salt solution (no $\text{Ca}^{2+}/\text{Mg}^{2+}$) to remove mucus before incubating in 2 ml dissociation media containing 2.4 U/ml Dispase II (Sigma) and 0.5% collagenase Type I (Sigma) in DMEM/F12 + GlutaMax (ThermoFisher) for 30-60 minutes at 37 °C. Following digestion, the tissue was triturated, first with a wide-bore fire-polished pipette (5x) then with a narrow-bore pipette (15-20x). Growth medium (DMEM/F-12 + GlutaMax, 10% FBS, 1% penicillin-streptomycin, 1% insulin-transferrin-selenium) was added, and the dissociated cells were centrifuged at 300 xg for 5 minutes. The supernatant was discarded and the cell pellet re-suspended in growth medium. The cell suspension was plated at varying densities (between 5,000 and 10,000 cells per coverslip) onto poly-L-lysine coated coverslips (100 µg/ml), and then maintained in a humidified incubator at 37 °C and 5% CO₂ for 1-3 days *in vitro* (DIV). For rat bulb OEC cultures, the two outermost layers of the olfactory bulb were digested in 1% trypsin (Worthington Biochemicals) in Hank's balanced salt solution (no $\text{Ca}^{2+}/\text{Mg}^{2+}$) at 37 °C for 10 minutes. Growth medium was added to quench the reaction, and the tissue was then allowed to settle at the bottom of the tube. All but ~1 ml of excess solution was removed and DNase I (400 U;

ThermoFisher) was added. The tissue was then triturated as described for the mucosal tissue. Growth media was added and the cells were centrifuged at 300 xg for 5 minutes. The supernatant was removed, and the cell pellet re-suspended in growth medium. The cell suspension was then plated and incubated as described for the mucosal cultures.

Electrophysiology. Whole-cell patch clamp recordings were performed at room temperature, using an Axopatch 200B amplifier and a Digidata board (Molecular Devices) under the control of pClamp acquisition software (version 8, Molecular Devices). Cells were superfused continuously with an external solution containing (in mM): 145 NaCl, 4 KCl, 1 MgCl₂, 1.3 CaCl₂, 10 HEPES and 5 glucose, pH 7.3. BaCl₂ and desipramine hydrochloride (Sigma) were prepared as 1 M and 100 mM stock solutions in water, respectively, before dilution in artificial perilymph solution to a final concentration of 100 μM. Patch pipettes were pulled from borosilicate glass (GC120TF-10, Harvard Apparatus) and had a resistance of 3-6.5 MΩ when filled with intracellular solution containing (in mM): 130 K-gluconate, 5 KCl, 2 MgATP, 2 Na₂ATP, 0.3 Na₃GTP, 10 Na₂-phosphocreatine, 1 EGTA and 10 HEPES, pH 7.2. In some recordings the internal solution was supplemented by 0.1% neurobiotin tracer (Vector Laboratories), and this was detected after fixation using fluorescently-tagged streptavidin (1:1000, added with secondary antibodies; Life Technologies), as described elsewhere (Jagger, Nickel, & Forge, 2014). Series resistance was compensated online by 70%. The liquid junction potential, measured at -13 mV, was subtracted offline. Resting membrane potential was measured using the $I=0$ circuitry of the amplifier. The voltage clamp protocol used to assess the currents is described in the Results section and Figure Legends. To enable comparison of the current-voltage relationship of individual cells, whole-cell currents were normalized to the maximum inward current for each cell. Cells were selected for recording based on their morphology (see Results), and data were analyzed if the recordings lasted through complete voltage clamp protocols or drug applications. All group data is expressed as mean ± standard error of the mean (SE). Data was obtained from four independent cultures for rat OM and rat OB experiments, and from three independent cultures for human OM experiments.

Tissue sectioning and immunofluorescence. Rat OB and OM were fixed in 4% paraformaldehyde (PFA) for overnight at 4 °C, and then mounted in 4% low-melting temperature agarose, before sectioning at 150 µm intervals on a vibratome (1000 plus system, Intracel). Tissues were not decalcified prior to sectioning. Cells cultured on coverslips were fixed in 4% PFA for 20 minutes at room temperature, and then stored in PBS. All steps in the immunofluorescence protocol were performed at room temperature. Sections and cells were blocked and permeabilized in 10% normal goat serum and 0.2% Triton-X-100 in PBS for 1 hour, and then incubated in primary antibodies diluted in lysine blocking solution (0.1 M lysine and 0.2% Triton-X-100 in PBS) for 3 hours, followed by three 10 minute washes in PBS. When using primary antibodies raised in goat, normal goat serum was substituted by FBS. Sections or cells were incubated in the secondary antibodies diluted 1:400 in lysine blocking solution for 1 hour, followed by three further washes in PBS. For imaging, sections were mounted in glass bottom dishes (MatTek Corporation) containing Vectashield mounting medium with DAPI (Vector Laboratories), whereas cells on coverslips were mounted on glass slides. Confocal images were acquired with a laser scanning confocal microscope (Carl Zeiss) equipped with 10x (N.A. 0.3), 20x (N.A. 0.75), and 63x (N.A. 1.2) objectives. The images shown are maximum intensity z-projections of 3-9 adjacent z-planes, except Figures 4b and 4c that are single z-planes.

Antibodies. The following primary antibodies were used for immunofluorescence: rabbit polyclonal anti-Kir4.1 (APC-035, Alomone Labs, RRID:AB_2040120); guinea pig polyclonal anti-Kir4.1 (AGP-012, Alomone Labs, RRID:AB_2340962); mouse monoclonal anti-βIII-tubulin (subtype IgG_{2a}; clone TUJ1; MMS-435P, Covance, RRID:AB_2313773); rabbit polyclonal anti-S100 (Z0311; Dako, RRID:AB_10013383); goat polyclonal anti-OMP (019-22291, Wako, RRID:AB_664696). Alexa Fluor-tagged secondary antibodies (Life Technologies) were used to detect primary antibodies: Alexa Fluor 488 goat anti-guinea pig (A-11073, RRID:AB_2534117); Alexa Fluor 633 goat anti-

mouse IgG_{2a} (A-21136, RRID:AB_2535775); Alexa Fluor 488 donkey anti-mouse (A-21202, RRID:AB_141607); Alexa Fluor 555 donkey anti-rabbit (A-31572, RRID:AB_162543); Alexa Fluor 633 donkey anti-goat (A-21082, RRID:AB_2535739).

Results

The main aim of this study was to determine the electrophysiological properties of cultured peripheral OECs. These experiments could enable us (1) to identify ion channel mechanisms that underlie their functions *in vivo*, and (2) identify protein markers that could help refine cell isolation procedures, and (3) to allow functional assessment of biopsied cells obtained for transplantation therapies. As a first part of this procedure, we studied the properties of cultured OECs from the rat OM and then OECs from the rat OB, which provided a first comparative analysis of these cells obtained from different regions. These experiments allowed us to determine the best conditions for effective cell isolations, and that our experimental conditions could maintain OECs appropriately for patch clamp recordings. With these conditions, we could then efficiently characterize the properties of OECs within valuable human OM biopsies.

OECs cultured from the rat olfactory mucosa display weak inwardly rectifying membrane currents

Using approaches previously described for human cells (Kachramanoglou et al., 2013), we prepared dissociated cell cultures of OECs harvested from the rat OM. These primary cultures provided a mixture of cell types following 1-3 DIV, some of which were identified positively as OECs due to their cytoplasmic and nuclear labelling with an anti-S100 antibody (S100+ cells; **Figure 1a**). S100+ cells had extensive multipolar cytoplasmic projections, or had an extended spindle-shaped morphology. Labelling of a minority of cells using a β III-tubulin antibody identified them as OSNs, and cells not labeled by either of the antibodies most likely represented resident populations of epithelial cells and/or fibroblasts. Whole-cell patch clamp recordings were also carried out following 1-3 DIV, and putative OECs were targeted (**Figure 1b**) based on characteristic morphologies identified by the S100 antibody labelling experiments. Given the possibility of intercellular gap junctional coupling, as reported for OECs in mouse OB (Rela et al., 2010), recordings avoided large groups of cells. In preliminary recordings, the patch pipette internal solution was supplemented with neurobiotin

(Jagger et al., 2014), which following paraformaldehyde fixation could be detected in cells confirmed as OECs by S100 labelling (**Figure 1c**). Dialysis of S100 from the cytoplasm during whole-cell recordings could be consistent with its presumed role as a soluble calcium-binding protein.

In response to a series of 200 ms voltage steps, a prominent subset of mucosal OECS (19/42 cells) displayed weak inwardly rectifying or non-rectifying currents (**Figure 2a-c**). Cells with these current profiles had hyperpolarized resting membrane potentials of -79.3 ± 0.9 mV ($n = 19$). $100 \mu\text{M}$ Ba^{2+} was applied to the bath solution to determine whether Kir channels mediated the weak inwardly rectifying currents, (**Figure 2d,e**). Ba^{2+} application resulted in a substantial block of the membrane currents (**Figure 2d,e**; control current amplitude at -153 mV = -3.28 ± 1.04 nA, Ba^{2+} current amplitude = -0.20 ± 0.09 nA, $n=7$). Ba^{2+} application caused a modest depolarization of the resting membrane potential that was reversible on washout (**Figure 2f**; control $V_m = -79.80 \pm 1.81$ mV, Ba^{2+} $V_m = -64.65 \pm 6.43$ mV, wash $V_m = -77.85 \pm 2.46$ mV, $n=6$). The digitally subtracted Ba^{2+} -sensitive currents displayed weak inward rectification (**Figure 2g,h**). Accordingly, the weak inwardly rectifying currents were also sensitive to the tricyclic anti-depressant desipramine ($100 \mu\text{M}$; **Figure 3a,b**; control current amplitude at -153 mV = -3.74 ± 1.02 nA, desipramine current amplitude = -0.48 ± 0.21 nA, $n=6$), a known blocker of Kir4-family channels (Su et al., 2007). Like Ba^{2+} , desipramine had a depolarizing effect on the resting membrane potential of the cells, which was reversible on washout (**Figure 3c**; control $V_m = -81.06 \pm 1.16$ mV, desipramine $V_m = -58.42 \pm 9.18$ mV, wash $V_m = -78.02 \pm 1.39$ mV, $n=5$). The kinetics and voltage-dependence of the digitally subtracted desipramine-sensitive whole-cell currents bore a strong resemblance to those blocked by Ba^{2+} (**Figure 3d,e**). Consistent with the effects of this blocker of Kir4-family channels, there was Kir4.1 immunofluorescence detected in S100+ OECs (**Figure 3f**).

Prompted by the similarities between these currents and those in other glial cells mediated by Kir4.1 channel subunits (Butt & Kalsi, 2006; Seifert, Henneberger, & Steinhauser, 2018; Tang,

Schmidt, Perez-Leighton, & Kofuji, 2010), we next used immunofluorescence to determine whether these subunits were expressed within OM tissue. In sections cut from the rat OM, S100+ OECs were in close association with OSN axons running through lamina propria (**Figure 4a,b**). The Kir4.1 antibody labelled these S100+ OECs (**Figure 4c**). Within each fasciculation, Kir4.1+ OECs surrounded axons labelled by the olfactory sensory neuron marker OMP (**Figure 4d**).

The membrane properties of peripheral and central OECs are different.

Previous studies in the mouse OB have reported that once gap junction channels are blocked, the OECs have non-linear current profiles (Rela et al., 2010; Rela et al., 2015). These responses point to variable contributions from strong inward rectifier and strong outward rectifier currents, distinct from the weak rectification profile we observed in OECs from the rat OM. To investigate possible differences in membrane properties of peripheral and central OECs, we next prepared cultures from the rat OB. In 16/23 cells (1-3 DIV) there was a strong inward rectification in response to hyperpolarizing voltage steps below -80 mV, and a strong outward rectification in response to depolarizing voltage steps above -40 mV (**Figure 5a-c**). In the presence of Ba²⁺, only strong outwardly rectifying currents remained (**Figure 5d,e**). The digitally subtracted Ba²⁺-sensitive inward currents displayed a strongly rectifying profile (**Figure 5f,g**), with little or no outward component at depolarized potentials (**Figure 5g**). Direct comparison of the mean Ba²⁺-sensitive currents in OECs derived from OB and OM clearly highlighted their contrasting properties (**Figure 5h**).

Given the apparent lack of weak rectifier currents in central OECs, we next carried out immunofluorescence using sections of rat OB. S100+ cells were evident in close association with OSN axons within the ONL, and within the GL (**Figure 6a**). In agreement with previous observations in rats (Higashi et al., 2001), Kir4.1 immuno-reactivity was largely absent from OECs within the ONL (**Figure 6a,b**). Diffuse Kir4.1 immunofluorescence was evident in S100+ cells within the glomeruli

though (**Figure 6a**), and within large multipolar cells at the border of the ONL and GL (**Figure 6b**). Together, these experiments demonstrate that ion channel expression in OECs is regionally specific, an observation that suggests these cells play different roles in the peripheral and central nervous tissue environments.

OECs cultured from the rat and human olfactory mucosa are functionally comparable.

Having validated our culturing and recording conditions using rat cells, in a final group of experiments we aimed to determine the electrophysiological profile of OECs harvested by endoscopic biopsies of human OM. In response to the same voltage step protocol applied to rat mucosal OECs (e.g. **Figure 2a**), a prominent subpopulation of human OECs (11/29, 1-3 DIV) displayed weak inwardly rectifying currents (**Figure 7a-c**). Cells with this type of current had hyperpolarized resting membrane potentials of -80.2 ± 1.0 mV ($n = 11$). $100 \mu\text{M Ba}^{2+}$ application resulted in a substantial block of the weak inwardly rectifying current (**Figure 7d,e**; control current amplitude at -153 mV = -1.32 ± 0.2 nA, Ba^{2+} current amplitude = -0.16 ± 0.04 nA, $n=6$). Ba^{2+} also caused a depolarization of the resting membrane potential of human OECs, which was reversible upon washout (**Figure 7f**; control $V_m = -81.42 \pm 1.36$ mV, $n=6$; Ba^{2+} $V_m = -54.63 \pm 3.74$ mV, $n=6$; wash $V_m = -79.08 \pm 1.32$ mV, $n=5$). The digitally subtracted Ba^{2+} -sensitive currents showed weak inward rectification (**Figure 7g,h**) and direct comparison of the Ba^{2+} -sensitive currents of OECs from human and rat OM revealed an almost complete overlap in their current-voltage relationship (**Figure 7h inset**). We did not identify Kir4.1+ OECs in fixed sections prepared from biopsies of human OM (not shown), but there was a sub-population of cells in the human OM cultures which were double labelled for S100 and Kir4.1 (**Figure 7i**), suggesting that Kir4.1 channels might mediate the weak inwardly rectifying currents.

Discussion

The main findings of this study are (1) that there are differences in the membrane physiology of OECs derived from the olfactory periphery and those that reside within the central nervous system (CNS), and (2) that OECs biopsied from the OM display membrane properties that are consistent with roles in K^+ homeostasis during the transduction of olfactory stimuli. These results should improve our understanding of the physiological roles played by these specialized glial cells during normal olfaction, and the description of distinct membrane properties within peripheral and central OECs may help explain how the two types of OECs behave when transplanted into the damaged or diseased CNS.

Our experiments reveal previously unrecognized qualities of OECs resident in the olfactory periphery. Whole-cell patch clamp recordings identified weak inward rectifier currents that were sensitive to both Ba^{2+} and desipramine, indicating a likely involvement of Kir4-family channel subunits. Ba^{2+} -sensitive currents in rat and human OECs from the OM had near-identical kinetics and voltage-dependence. The reversible depolarization of the resting membrane potential during pharmacological block suggests that these currents contribute to the hyperpolarised resting membrane potential of OECs. A similar role for weak inwardly rectifying channels has been proposed for astrocytes (Butt & Kalsi, 2006) and satellite glial cells (Tang et al., 2010). The expression of these channels in glia has been associated with the maintenance of physiological levels of K^+ within the extracellular space, particularly during periods of high neuronal activity in the CNS (Bay & Butt, 2012; Butt & Kalsi, 2006; Higashi et al., 2001). Satellite glial cells in peripheral ganglia also express these weakly rectifying channels at high densities, suggesting comparable homeostatic roles support afferent signaling within various sensory modalities (Hibino et al., 1999; Tang et al., 2010).

The patch clamp data prompted our subsequent detection of Kir4.1 channel subunits within rat OECs lying in close association with the unmyelinated axons of OSNs. S100+/Kir4.1+ OECs were evident within the centrally directed axonal bundles running within lamina propria. Unfortunately, in the present study we were unable to obtain consistent Kir4.1 immunofluorescence from sections derived from the human OM. The reasons for this are currently unclear, but this may have been due to limitations of the fixation achievable in the biopsied human tissue. However, consistent with the electrophysiology experiments, in human OM cultures we were able to identify cultured S100+ cells that were also immuno-positive for Kir4.1.

In agreement with earlier studies in mice (Rela et al., 2015) and rats (Higashi et al., 2001), we did not detect Kir4.1 immunofluorescence within the ONL of the rat OB, where OECs lie adjacent to OSN axons. Accordingly, under the same *in vitro* maintenance and experimental conditions that we observed weak inwardly rectifying currents in a sub-population of OECs from the rat OM, the currents in OECs derived from the rat OB did not show weak rectification. In common with previous observations from some OECs in the mouse OB (Rela et al., 2015), the Ba²⁺-sensitive currents found here in the majority (16/23) of OECs from the rat OB displayed strong inward rectification, suggesting a contribution by Kir channels with different properties to those of Kir4.1. The molecular identity of these channels remains undetermined. In this majority group of cells, there were also Ba²⁺-insensitive outwardly rectifying currents. We did not investigate the basis of any heterogeneity in the membrane properties of rat central OECs, which has been described extensively elsewhere (Rela et al., 2010; Rela et al., 2015). The biological importance of this heterogeneity remains to be determined. We cannot completely rule out a contribution from this heterogeneity within the central OEC population, or any differences in the purity of our cultures from OM and OB, to the clear distinction in the electrophysiological properties of OECs from the two sources. However, given the absence of Kir4.1 immunofluorescence in the ONL shown here, and by others (Higashi et al., 2001; Rela et al., 2015), it seems likely the observed electrophysiological differences may be explained by regional variations in ion channel expression.

Large Kir4.1+ cells were evident within the OB deeper layers where OSNs relay with projection neurons. Although we did not confirm their identity, these may be astrocytes known to extend their processes into the synaptic regions within the glomeruli (Raisman, 2001). A population of multipolar glia double-labelled for Kir4.1 and the astrocytic marker glial fibrillary acidic protein (GFAP) have been previously located within the glomerular layer of the rat OB (Higashi et al., 2001). The continuous Kir4.1 labelling within the OM, but not within the ONL, suggests that Kir4.1 subunits contribute only to OEC function in the periphery. Indeed, the distinct regional properties of the OECs recorded in this study, which reflect the differences in their expression of K⁺ channel subunits, point to fundamentally contrasting physiological roles for glia in the olfactory periphery and the brain.

The homeostasis and regeneration of neurons often relies on a bi-directional communication that informs the attendant glia of ongoing neural activity. Studies using OB slice preparations have revealed glutamatergic and purinergic receptor-mediated signaling between OSN axons and OECs (Rieger et al., 2007). This metabotropic mechanism involves a contribution from intracellular Ca²⁺ stores (Hayat et al., 2003), Ca²⁺ influx channels (Davies, Hayat, Wigley, & Robbins, 2004), and intracellular Ca²⁺ waves mediated by gap junctions (Stavermann et al., 2015). There is evidence of several connexins expressed by the non-neuronal cells in the OB (Rash et al., 2005), and genetic deletion of Cx43 leads to the loss of intercellular gap junctional coupling between OECs (Piantanida et al., 2019). There is less known about the physiology of peripheral OECs. Our whole-cell recordings have now revealed potential roles for weakly rectifying K⁺ channels in the normal function of the olfactory periphery. A consequence of this finding is that we might now consider Kir4.1 as a functional marker of OECs within this tissue, both in experimental animal studies and within tissues excised from humans. It remains to be determined though, whether Kir4.1 expression is detectable within the intact human OM, as our experiments here did not clearly demonstrate it. If Kir4.1 does contribute to normal homeostasis of OSNs, this may have consequences for our understanding of

certain forms of anosmia, and of genetic conditions in humans such as EAST syndrome (Bockenhauer et al., 2009), in which sensory deficits result from mutations of the gene coding for Kir4.1 protein.

The continual turnover of OSNs during normal olfactory function demonstrates the potential for OECs to repair axonal damage in the human CNS. The answer to how OECs promote neuronal regeneration and regrowth of their axons may be multi-factorial. There is evidence for several mechanisms mediated by transplanted peripheral and central OECs. These include neuroprotection and increased axonal sprouting (Li, Field, & Raisman, 1997; Novikova, Lobov, Wiberg, & Novikov, 2011; Ramon-Cueto, Plant, Avila, & Bunge, 1998; Richter, Fletcher, Liu, Tetzlaff, & Roskams, 2005), recruitment of other beneficial cell types (Richter et al., 2005), remyelination (Franklin, Gilson, Franceschini, & Barnett, 1996; Imaizumi, Lankford, Waxman, Greer, & Kocsis, 1998; Radtke et al., 2004), and modification of the glial scar (Ramer et al., 2004). Due to the lower risk and invasiveness of the procedure, some researchers prefer biopsy of OECs from the OM rather than from the OB (Choi & Gladwin, 2015; Yao et al., 2018). These cells may have additional advantages brought about by their increased proliferative abilities (Jani & Raisman, 2004), and a greater capacity for migration and axonal growth (Richter et al., 2005). Further comparative studies of OECs from the OM and OB will be required to unravel the physiological differences between them, and to explain potential variability in their regenerative capacity.

Despite numerous reports of success following OEC transplantation into the CNS, there are also a number of studies with variable or negative outcomes. These may be a consequence of the discrepancies in the experiments and methods of assessment. The site of origin, the composition of cultures and their proliferative state may also be crucial factors that determine success following transplantation, and these have been reviewed recently elsewhere (Assinck et al., 2017; Gladwin & Choi, 2015; Gomez et al., 2018). The regenerative capacity of OECs may be determined by the

length of time that they are cultured prior to transplantation. OECs cultured for short periods were more successful in terms of neuroprotection and growth sprouting than those maintained for longer *in vitro* before transplantation (Novikova et al., 2011). Our results suggest that OECs cultured from both rat and human OM continue to express weak rectifier channels following their excision from the olfactory periphery. This observation may be relevant to the question of their proliferative state in culture. Pharmacological block of weak inwardly rectifying currents in quiescent astrocytes causes increased proliferation, and results in an increased proportion of cells in S-phase (Higashimori & Sontheimer, 2007). Ion channels expressed in cultured OECs could determine their proliferative state, and thus determine their likelihood of achieving both the growth in cell numbers and the de-differentiation required to maximize regeneration after transplantation.

Our work has provided a platform for future studies of biopsied human peripheral OECs *in vitro*. It has demonstrated a functional distinction between the OECs of the olfactory periphery and those within the brain. It has indirectly identified the Kir4.1 channel subunit as a functional biomarker for peripheral OECs, potentially enabling their identification within OM endoscopic biopsies where numerous cell types are unavoidably present. This finding may help refine methods for their purification. Our study also verifies the adult rat OM as an experimental model for characterizing the physiology of human OECs. Further studies utilizing more intact preparations will be required to delineate the complex physiological roles of OECs within the normal olfactory system, and their interactions with neuronal axons in the periphery. Subsequently, we may gain a better understanding of how the membrane proteins underlying these normal processes change their expression following excision of OECs from the nasal mucosa. By targeting specific ion channel mechanisms and manipulating the membrane physiology of cultured OECs, we may be able to modulate the regenerative capacity of these cells for transplantation therapies.

Figure Legends

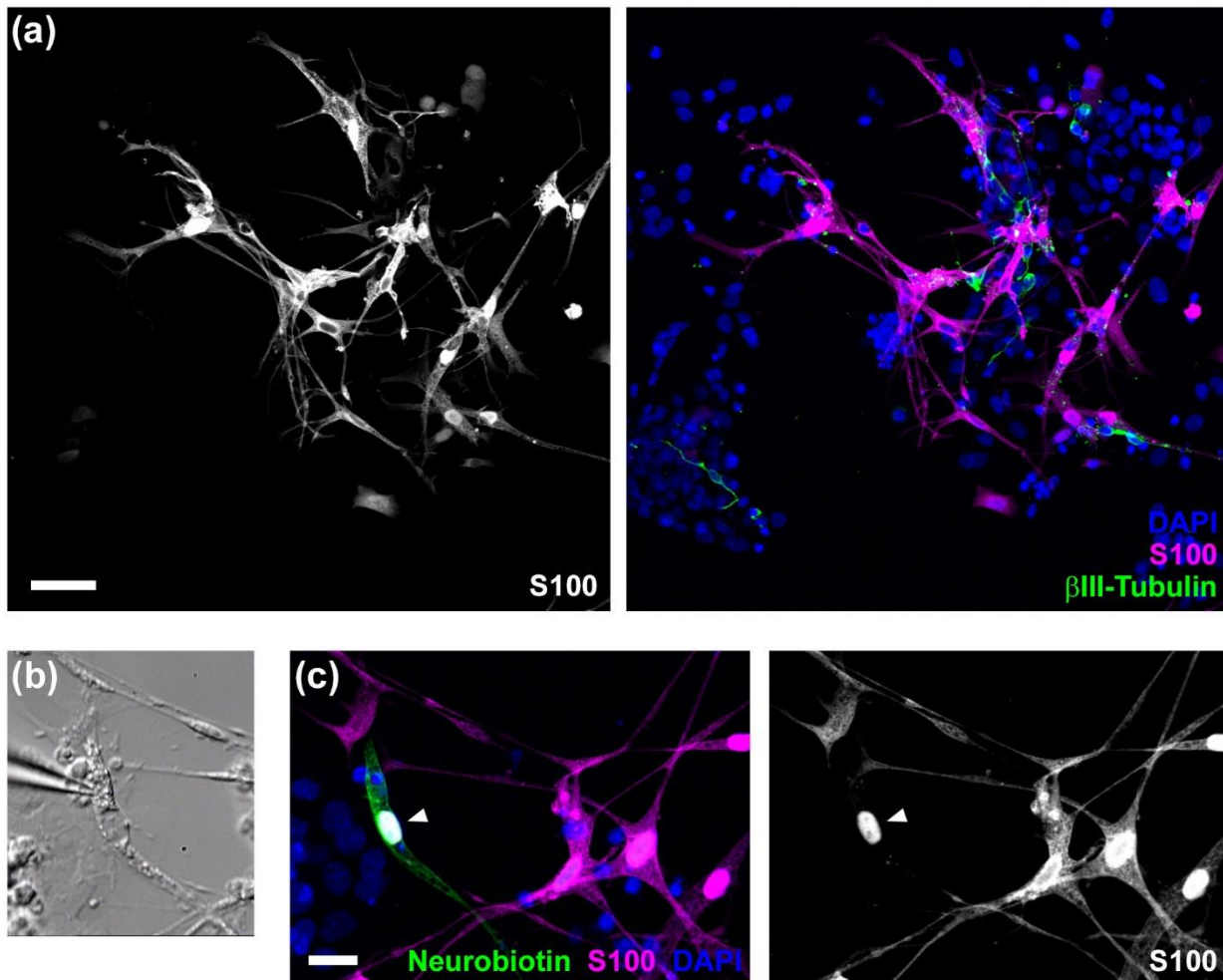


Figure 1. Identification of S100+ OECs cultured from the rat olfactory mucosa. (a) Immunofluorescent labelling of cultured cells following 2 DIV. Sub-populations of cells were identified as OECs (labelled by anti-S100, magenta), or OSNs (labelled by anti- β III-tubulin, green). Cell nuclei were labelled using DAPI (blue). Some cells were not labelled by either antibody. (b) Differential interference contrast (DIC) video-micrograph taken during a whole-cell recording carried out from a spindle-shaped cell. (c) Neurobiotin-streptavidin fluorescence (green) allowed identification of the spindle-shaped cell in (b) after fixation. S100 immunofluorescence (magenta) was co-detected in the nucleus of the dye-labelled cell (arrowhead). Scale bars: (a) 50 μ m, (c) 20 μ m.

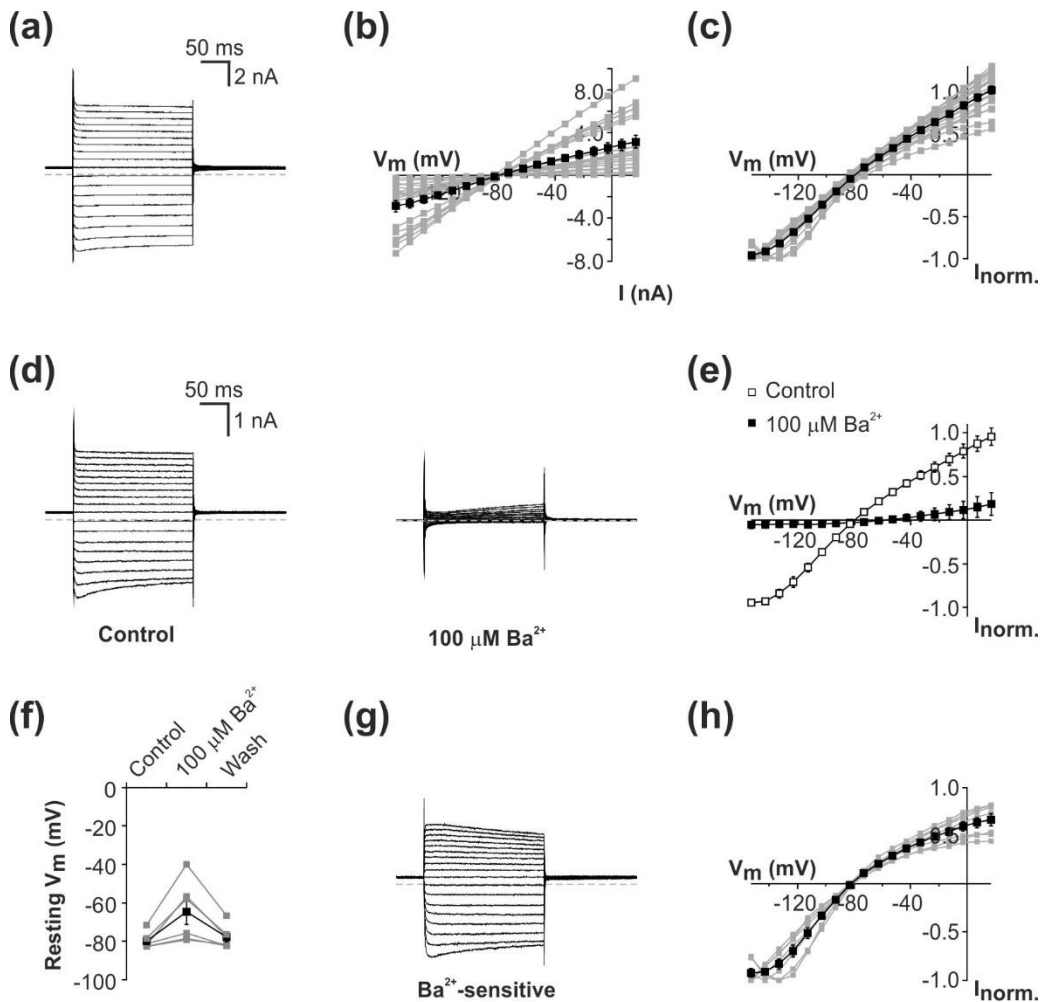


Figure 2. Weak rectifier currents in OECs cultured from the rat olfactory mucosa. (a) Whole-cell voltage clamp recording from an OEC following 3 DIV, showing membrane currents activated by sequential 200 ms voltage steps between -153 mV and 17 mV, in 10 mV increments from a holding potential of -73 mV. The discontinuous line denotes the position of zero-current. Hyperpolarizing steps activated large inward currents, whereas depolarizing steps typically activated outward currents. (b) Group (mean \pm SE, black squares) and individual (gray squares) current-voltage (I - V) relationships of 19 OECs after 1-3 DIV. (c) Normalized group and individual I - V plots demonstrated the weak voltage-dependence of the whole-cell currents. (d) Currents in a representative OEC before (control) and after bath application of 100 μ M Ba^{2+} . (e) Group I - V relationships before (open squares) and after (filled squares) Ba^{2+} application in seven OECs. (f) Bath applied Ba^{2+} depolarized the resting membrane potential (V_m) of all cells reversibly ($n = 6$). (g) Digital subtraction of the currents in the presence of Ba^{2+} from control currents revealed a weak

inwardly rectifying Ba^{2+} -sensitive current. (h) Group (black squares) and individual (gray squares) I - V relationships of Ba^{2+} -sensitive current in seven OECs.

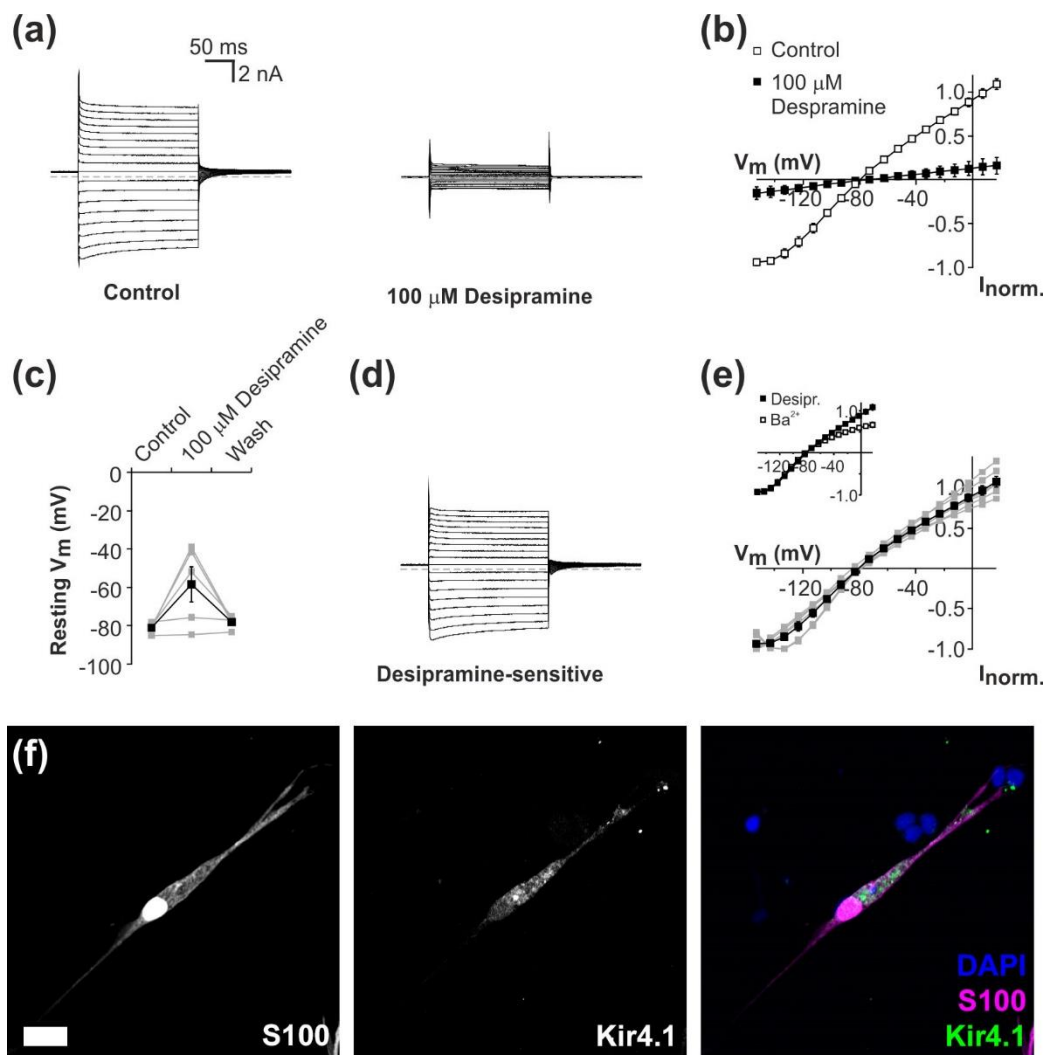


Figure 3. Weakly rectifying currents in rat olfactory mucosa OECs are sensitive to the Kir4 blocker desipramine. (a) Currents in a representative OEC before (control) and after bath application of 100 μM desipramine. (b) Group I - V relationships before (open squares) and after (filled squares) desipramine application in six OECs. (c) Bath applied desipramine depolarized the resting membrane potential (V_m) of 4/5 cells reversibly. (d) Digital subtraction of the currents in the presence of desipramine from control currents revealed a weak inwardly rectifying desipramine-sensitive current. (e) Group (black squares) and individual (gray squares) I - V relationships of desipramine-sensitive currents in six OECs. *Inset*, comparison of the Ba^{2+} -sensitive and desipramine-sensitive components of membrane currents recorded in OECs from rat OM (group data shown in Figure 2h and Figure 3e, respectively). (f) Immunofluorescence for S100 (magenta) and Kir4.1 (green) in a spindle-shaped cell. Nuclei labelled using DAPI (blue). Scale bar: 20 μm .

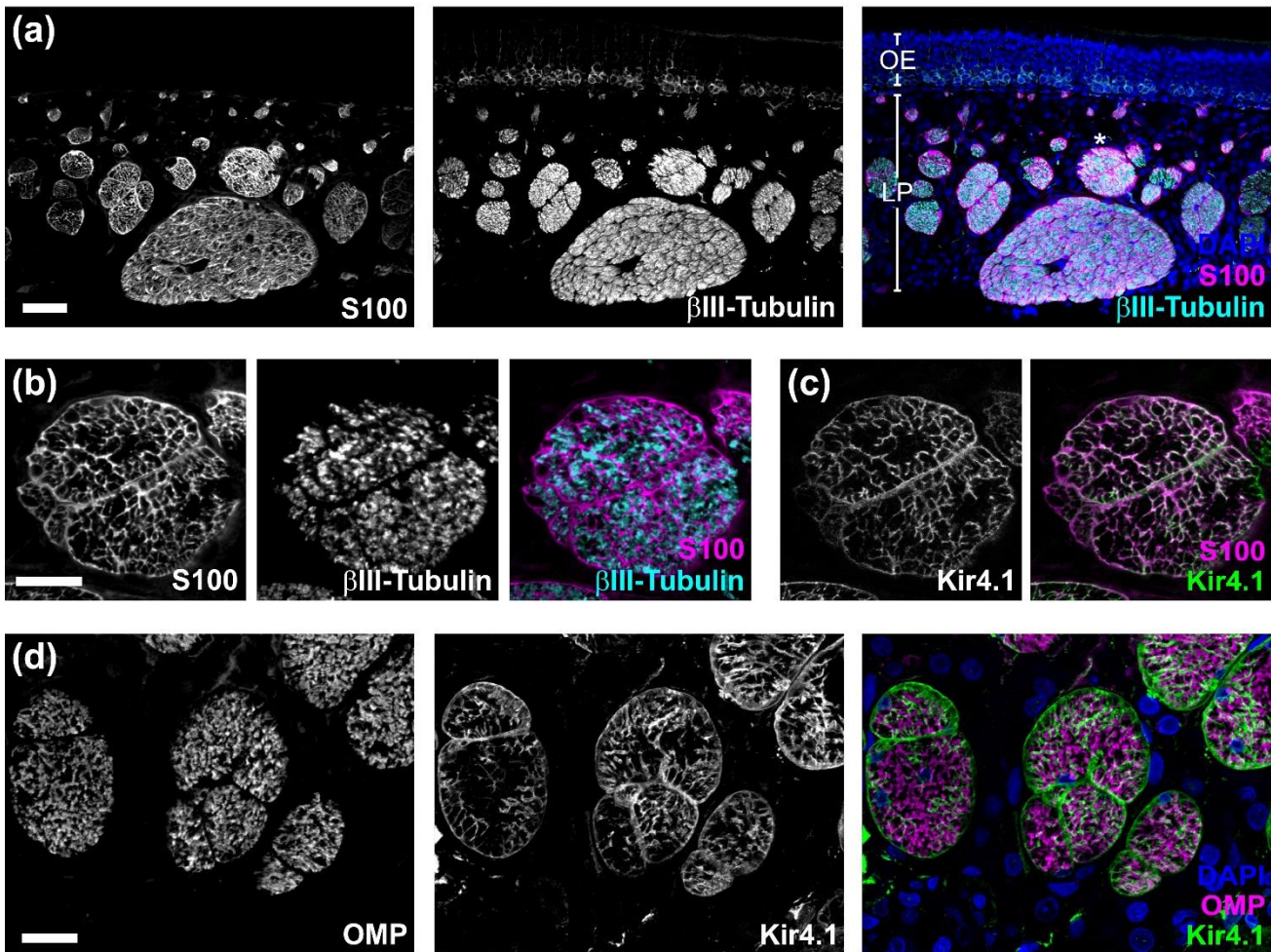


Figure 4. OECs in the rat olfactory mucosa express Kir4.1 channel subunits. (a) Horizontal section of rat OM, immuno-labelled for the OEC marker S100 (*left*) and the neuronal marker β III-tubulin (*center*). The overlay has cell nuclei counter-stained using DAPI (*right*). The cell bodies of OSNs reside within the olfactory epithelium (OE), and their axons fasciculate within lamina propria (LP). S100+ OECs lie beneath the basement membrane and in close association with OSN axons. (b-c) Detail of a fascicle highlighted in (a) (*), labelled for S100 and β III-tubulin (b), and for the weakly rectifying K⁺ channel subunit Kir4.1 (c). (d) Detail of fascicles where OSN axons are labelled using anti-OMP and OECs are labelled using anti-Kir4.1. Scale bars: (a) 50 μ m, (b-d) 20 μ m.

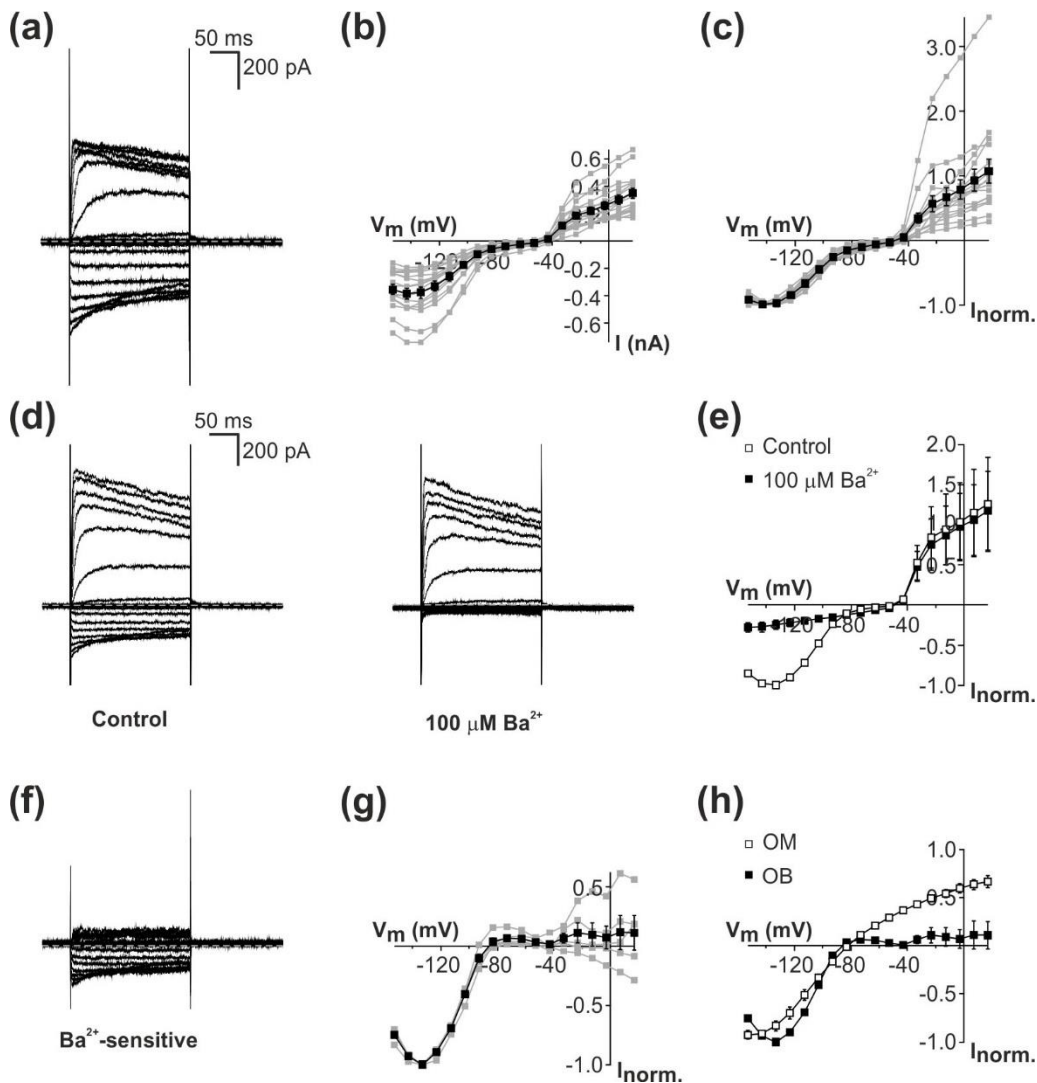


Figure 5. Membrane properties of OECs from the rat olfactory bulb are different to those from the rat olfactory mucosa. (a) Whole-cell voltage clamp recording from a representative OEC following 3 DIV, showing membrane currents activated by sequential 200 ms voltage steps between -153 mV and 17 mV, in 10 mV increments from a holding potential of -73 mV. Hyperpolarizing steps below around -80 mV activated inward currents, whereas depolarizing steps above -40 mV typically activated smaller outward currents. (b) Group (mean \pm SE, black squares) and individual (gray squares) current-voltage (I - V) relationships of 16 OECs at 1-3 DIV. (c) Normalized I - V plots demonstrated the pronounced voltage-dependence of both inward and outward currents. (d) Currents before (control) and after bath application of 100 μ M Ba^{2+} in a representative OEC. (e) Group I - V relationships before (open squares) and after (filled squares) Ba^{2+} application ($n = 5$). (f) Digital subtraction of the currents in the presence of Ba^{2+} from control currents revealed a strong inwardly rectifying Ba^{2+} -sensitive current. (g) Group (black squares) and individual (gray

squares) *I-V* relationships of Ba²⁺-sensitive current in five OECs. (h) Comparison of the Ba²⁺-sensitive component of membrane currents recorded in OECs from rat OB and OM (group data shown in Figure 5g and Figure 2h, respectively).

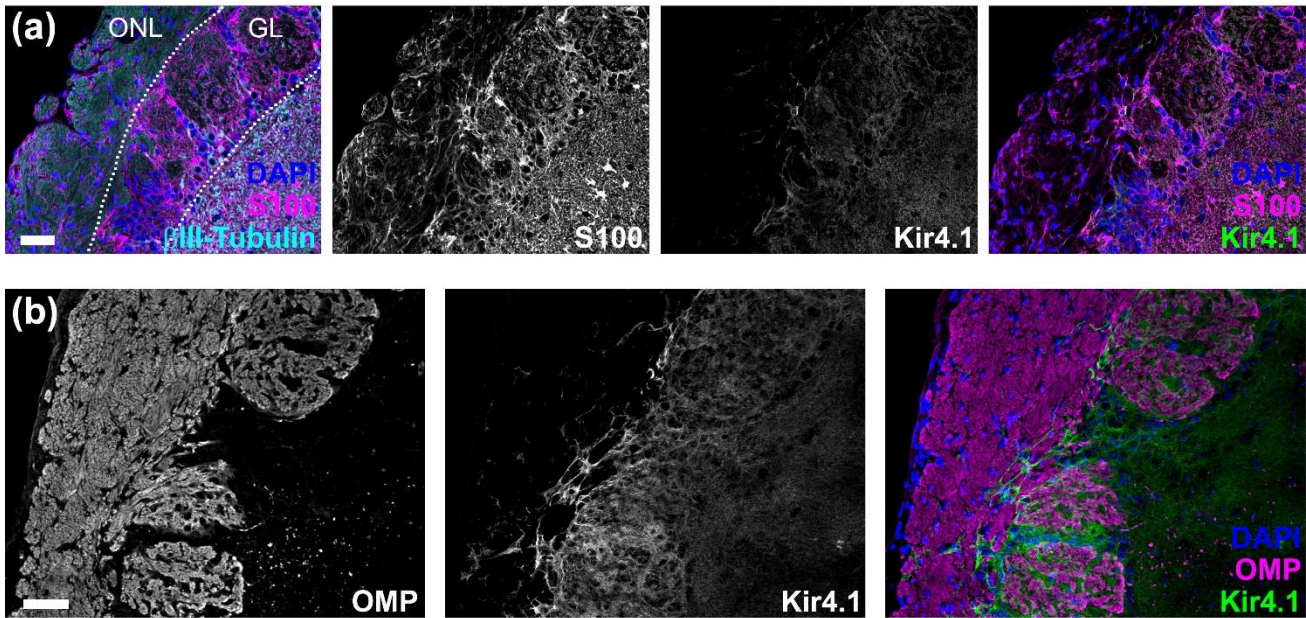


Figure 6. OECs in the outer olfactory nerve layer of the rat olfactory bulb lack expression of Kir4.1. (a) Sagittal section of rat OB showing OSN axons (labelled for the neuronal marker β III-tubulin) running through the outer nerve layer (ONL), before entering the glomerular layer (GL). Glial cells, including OECs in the ONL, are immuno-labelled for S100. Kir4.1 immunofluorescence was largely undetectable in the ONL, but was evident in cells of the deeper layers. The overlays have cell nuclei counter-stained using DAPI. (b) A different sagittal section of rat OB, immuno-labelled for the OSN marker OMP and Kir4.1. Kir4.1 immunofluorescence was largely undetectable in the ONL, and was restricted to large multi-polar cells within the GL. The overlay has cell nuclei counter-stained using DAPI. Scale bars: 50 μ m.

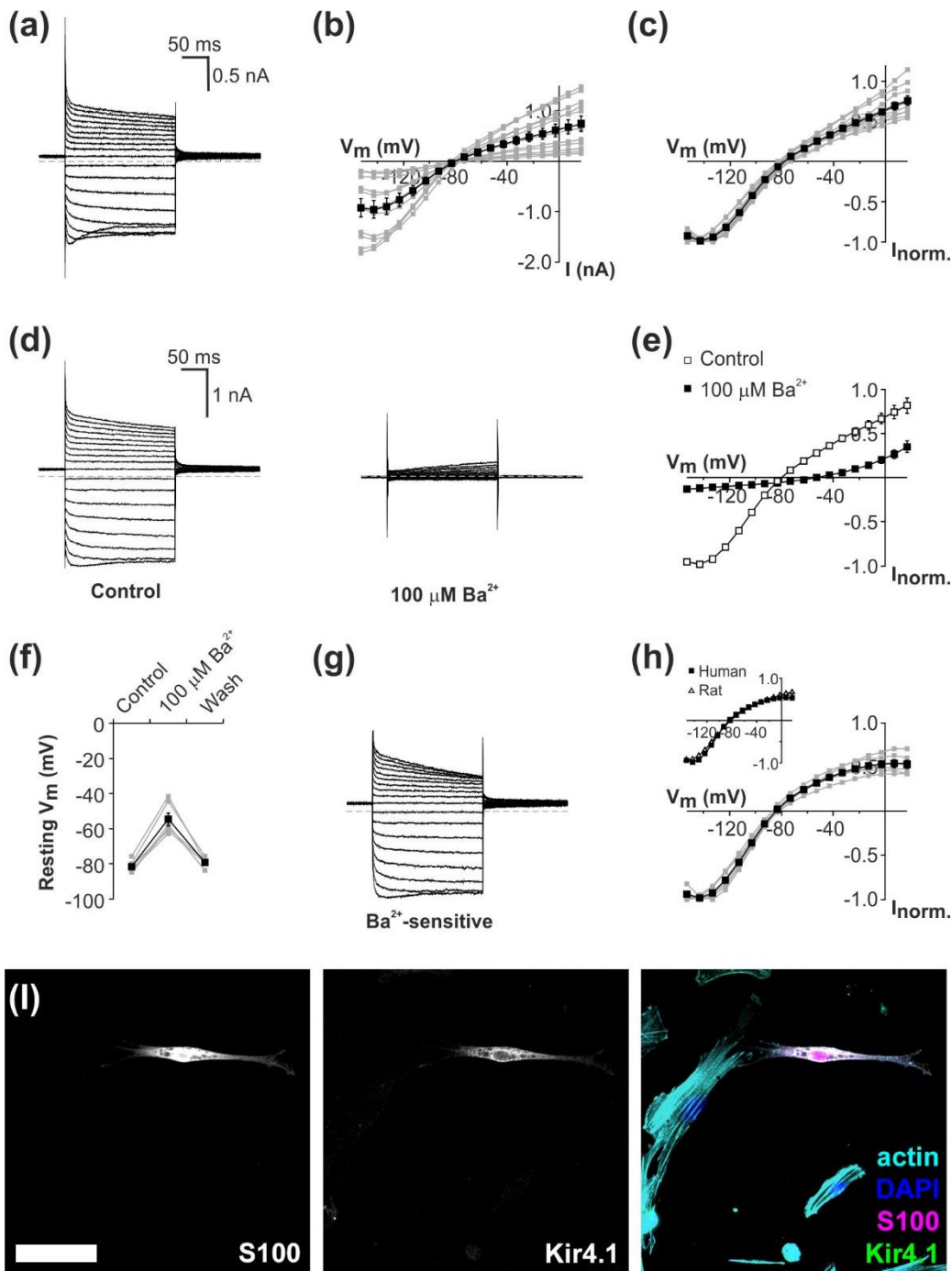


Figure 7. Membrane properties of OECs from the human olfactory mucosa are comparable to those from the rat olfactory mucosa. (a) Whole-cell voltage clamp recording from a representative human OEC following 3 DIV, showing membrane currents activated by sequential 200 ms voltage steps between -153 mV and 17 mV, in 10 mV increments from a holding potential of -73 mV. Hyperpolarizing steps activated large inward currents, whereas depolarizing steps typically activated outward currents. (b) Group (black squares) and individual (gray squares) $I-V$ relationships of 11 human OECs after 1-3 DIV. (c) Normalized group and individual $I-V$ plots demonstrated the weak voltage-dependence of the whole-cell currents. (d) Currents in a

representative human OEC before (control) and after bath application of 100 μM Ba^{2+} . (e) Group *I-V* relationships before (open squares) and after (filled squares) Ba^{2+} application in 6 OECs. (f) Bath applied Ba^{2+} depolarized the resting membrane potential (V_m) of all cells reversibly. (g) Digital subtraction of the currents in the presence of Ba^{2+} from control currents revealed a weak inwardly rectifying Ba^{2+} -sensitive current. (h) Group (black squares) and individual (gray squares) *I-V* relationships of Ba^{2+} -sensitive currents in six OECs. *Inset*, comparison of the Ba^{2+} -sensitive component of whole-cell currents recorded in OECs from human OM and rat OM (group data shown in Figure 7h and Figure 2h, respectively). (i) In a 3 DIV culture, a spindle-shaped cell co-labeled with anti-S100 (*left panel*) and anti-Kir4.1 antibodies (*center*). The overlay (*right*) has cell nuclei counter-stained using DAPI (blue), and F-actin using phalloidin (cyan). Scale bar: 50 μm .

Data Availability Statement

The data that support the findings of this study are available from the corresponding author upon reasonable request.

References

- Andrews, P. J., Poirrier, A. L., Lund, V. J., & Choi, D. (2016). Safety of human olfactory mucosal biopsy for the purpose of olfactory ensheathing cell harvest and nerve repair: a prospective controlled study in patients undergoing endoscopic sinus surgery. *Rhinology*, *54*(2), 183-191. doi:10.4193/Rhin15.365
- Assinck, P., Duncan, G. J., Hilton, B. J., Plemel, J. R., & Tetzlaff, W. (2017). Cell transplantation therapy for spinal cord injury. *Nat Neurosci*, *20*(5), 637-647. doi:10.1038/nn.4541
- Bay, V., & Butt, A. M. (2012). Relationship between glial potassium regulation and axon excitability: a role for glial Kir4.1 channels. *Glia*, *60*(4), 651-660. doi:10.1002/glia.22299
- Bockenbauer, D., Feather, S., Stanescu, H. C., Bandulik, S., Zdebik, A. A., Reichold, M., . . . Kleta, R. (2009). Epilepsy, ataxia, sensorineural deafness, tubulopathy, and KCNJ10 mutations. *N Engl J Med*, *360*(19), 1960-1970. doi:360/19/1960 [pii]
- 10.1056/NEJMoa0810276
- Brann, J. H., & Firestein, S. J. (2014). A lifetime of neurogenesis in the olfactory system. *Front Neurosci*, *8*, 182. doi:10.3389/fnins.2014.00182
- Butt, A. M., & Kalsi, A. (2006). Inwardly rectifying potassium channels (Kir) in central nervous system glia: a special role for Kir4.1 in glial functions. *J Cell Mol Med*, *10*(1), 33-44.
- Chen, C. R., Kachramanoglou, C., Li, D., Andrews, P., & Choi, D. (2014). Anatomy and cellular constituents of the human olfactory mucosa: a review. *J Neurol Surg B Skull Base*, *75*(5), 293-300. doi:10.1055/s-0033-1361837
- Choi, D., & Gladwin, K. (2015). Olfactory ensheathing cells: Part II--source of cells and application to patients. *World Neurosurg*, *83*(2), 251-256. doi:10.1016/j.wneu.2013.07.016
- Choi, D., Law, S., Raisman, G., & Li, D. (2008). Olfactory ensheathing cells in the nasal mucosa of the rat and human. *Br J Neurosurg*, *22*(2), 301-302. doi:10.1080/02688690701883442
- Davies, R., Hayat, S., Wigley, C. B., & Robbins, J. (2004). The calcium influx pathway in rat olfactory ensheathing cells shows TRPC channel pharmacology. *Brain Res*, *1023*(1), 154-156. doi:10.1016/j.brainres.2004.07.032
- de Castro, F. (2009). Wiring Olfaction: The Cellular and Molecular Mechanisms that Guide the Development of Synaptic Connections from the Nose to the Cortex. *Front Neurosci*, *3*, 52. doi:10.3389/neuro.22.004.2009
- Ekberg, J. A., & St John, J. A. (2014). Crucial roles for olfactory ensheathing cells and olfactory mucosal cells in the repair of damaged neural tracts. *Anat Rec (Hoboken)*, *297*(1), 121-128. doi:10.1002/ar.22803

- Franklin, R. J., Gilson, J. M., Franceschini, I. A., & Barnett, S. C. (1996). Schwann cell-like myelination following transplantation of an olfactory bulb-ensheathing cell line into areas of demyelination in the adult CNS. *Glia*, 17(3), 217-224. doi:10.1002/(SICI)1098-1136(199607)17:3<217::AID-GLIA4>3.0.CO;2-Y
- Garcia-Gonzalez, D., Murcia-Belmonte, V., Clemente, D., & De Castro, F. (2013). Olfactory system and demyelination. *Anat Rec (Hoboken)*, 296(9), 1424-1434. doi:10.1002/ar.22736
- Gladwin, K., & Choi, D. (2015). Olfactory ensheathing cells: part I-current concepts and experimental laboratory models. *World Neurosurg*, 83(1), 114-119. doi:10.1016/j.wneu.2013.03.010
- Gomez, R. M., Sanchez, M. Y., Portela-Lomba, M., Ghotme, K., Barreto, G. E., Sierra, J., & Moreno-Flores, M. T. (2018). Cell therapy for spinal cord injury with olfactory ensheathing glia cells (OECs). *Glia*, 66(7), 1267-1301. doi:10.1002/glia.23282
- Guerout, N., Derambure, C., Drouot, L., Bon-Mardion, N., Duclos, C., Boyer, O., & Marie, J. P. (2010). Comparative gene expression profiling of olfactory ensheathing cells from olfactory bulb and olfactory mucosa. *Glia*, 58(13), 1570-1580. doi:10.1002/glia.21030
- Hayat, S., Wigley, C. B., & Robbins, J. (2003). Intracellular calcium handling in rat olfactory ensheathing cells and its role in axonal regeneration. *Mol Cell Neurosci*, 22(2), 259-270.
- Hibino, H., Horio, Y., Fujita, A., Inanobe, A., Doi, K., Gotow, T., . . . Kurachi, Y. (1999). Expression of an inwardly rectifying K(+) channel, Kir4.1, in satellite cells of rat cochlear ganglia. *Am J Physiol*, 277(4), C638-644. doi:10.1152/ajpcell.1999.277.4.C638
- Higashi, K., Fujita, A., Inanobe, A., Tanemoto, M., Doi, K., Kubo, T., & Kurachi, Y. (2001). An inwardly rectifying K(+) channel, Kir4.1, expressed in astrocytes surrounds synapses and blood vessels in brain. *Am J Physiol Cell Physiol*, 281(3), C922-931. doi:10.1152/ajpcell.2001.281.3.C922
- Higashimori, H., & Sontheimer, H. (2007). Role of Kir4.1 channels in growth control of glia. *Glia*, 55(16), 1668-1679. doi:10.1002/glia.20574
- Honore, A., Le Corre, S., Derambure, C., Normand, R., Duclos, C., Boyer, O., . . . Guerout, N. (2012). Isolation, characterization, and genetic profiling of subpopulations of olfactory ensheathing cells from the olfactory bulb. *Glia*, 60(3), 404-413. doi:10.1002/glia.22274
- Hummel, T., Kobal, G., Gudziol, H., & Mackay-Sim, A. (2007). Normative data for the "Sniffin' Sticks" including tests of odor identification, odor discrimination, and olfactory thresholds: an upgrade based on a group of more than 3,000 subjects. *Eur Arch Otorhinolaryngol*, 264(3), 237-243. doi:10.1007/s00405-006-0173-0

- Imaizumi, T., Lankford, K. L., Waxman, S. G., Greer, C. A., & Kocsis, J. D. (1998). Transplanted olfactory ensheathing cells remyelinate and enhance axonal conduction in the demyelinated dorsal columns of the rat spinal cord. *J Neurosci*, *18*(16), 6176-6185.
- Jafek, B. W. (1983). Ultrastructure of human nasal mucosa. *Laryngoscope*, *93*(12), 1576-1599.
- Jagger, D. J., Nickel, R., & Forge, A. (2014). Gap junctional coupling is essential for epithelial repair in the avian cochlea. *J Neurosci*, *34*(48), 15851-15860. doi:10.1523/JNEUROSCI.1932-14.2014
- Jani, H. R., & Raisman, G. (2004). Ensheathing cell cultures from the olfactory bulb and mucosa. *Glia*, *47*(2), 130-137. doi:10.1002/glia.20038
- Kachramanoglou, C., Law, S., Andrews, P., Li, D., & Choi, D. (2013). Culture of olfactory ensheathing cells for central nerve repair: the limitations and potential of endoscopic olfactory mucosal biopsy. *Neurosurgery*, *72*(2), 170-178; discussion 178-179. doi:10.1227/NEU.0b013e31827b99be
- Li, Y., Field, P. M., & Raisman, G. (1997). Repair of adult rat corticospinal tract by transplants of olfactory ensheathing cells. *Science*, *277*(5334), 2000-2002.
- Liu, K., Li, Y., Wang, H., Jiang, X., Zhao, Y., Sun, D., . . . Zhou, C. (2010). The immunohistochemical characterization of human fetal olfactory bulb and olfactory ensheathing cells in culture as a source for clinical CNS restoration. *Anat Rec (Hoboken)*, *293*(3), 359-369. doi:10.1002/ar.21030
- Neumann, C., Tsioulos, K., Merkonidis, C., Salam, M., Clark, A., & Philpott, C. (2012). Validation study of the "Sniffin' Sticks" olfactory test in a British population: a preliminary communication. *Clin Otolaryngol*, *37*(1), 23-27. doi:10.1111/j.1749-4486.2012.02431.x
- Novikova, L. N., Lobov, S., Wiberg, M., & Novikov, L. N. (2011). Efficacy of olfactory ensheathing cells to support regeneration after spinal cord injury is influenced by method of culture preparation. *Exp Neurol*, *229*(1), 132-142. doi:10.1016/j.expneurol.2010.09.021
- Oprych, K., Cotfas, D., & Choi, D. (2017). Common olfactory ensheathing glial markers in the developing human olfactory system. *Brain Struct Funct*, *222*(4), 1877-1895. doi:10.1007/s00429-016-1313-y
- Piantanida, A. P., Acosta, L. E., Brocardo, L., Capurro, C., Greer, C. A., & Relva, L. (2019). Selective Cre-mediated gene deletion identifies connexin 43 as the main connexin channel supporting olfactory ensheathing cell networks. *J Comp Neurol*. doi:10.1002/cne.24628
- Radtke, C., Akiyama, Y., Brokaw, J., Lankford, K. L., Wewetzer, K., Fodor, W. L., & Kocsis, J. D. (2004). Remyelination of the nonhuman primate spinal cord by transplantation of H-transferase transgenic adult pig olfactory ensheathing cells. *FASEB J*, *18*(2), 335-337. doi:10.1096/fj.03-0214fje
- Raisman, G. (2001). Olfactory ensheathing cells - another miracle cure for spinal cord injury? *Nat Rev Neurosci*, *2*(5), 369-375. doi:10.1038/35072576

- Ramer, L. M., Au, E., Richter, M. W., Liu, J., Tetzlaff, W., & Roskams, A. J. (2004). Peripheral olfactory ensheathing cells reduce scar and cavity formation and promote regeneration after spinal cord injury. *J Comp Neurol*, *473*(1), 1-15. doi:10.1002/cne.20049
- Ramon-Cueto, A., Plant, G. W., Avila, J., & Bunge, M. B. (1998). Long-distance axonal regeneration in the transected adult rat spinal cord is promoted by olfactory ensheathing glia transplants. *J Neurosci*, *18*(10), 3803-3815.
- Rash, J. E., Davidson, K. G., Kamasawa, N., Yasumura, T., Kamasawa, M., Zhang, C., . . . Nagy, J. I. (2005). Ultrastructural localization of connexins (Cx36, Cx43, Cx45), glutamate receptors and aquaporin-4 in rodent olfactory mucosa, olfactory nerve and olfactory bulb. *J Neurocytol*, *34*(3-5), 307-341. doi:10.1007/s11068-005-8360-2
- Rela, L., Bordey, A., & Greer, C. A. (2010). Olfactory ensheathing cell membrane properties are shaped by connectivity. *Glia*, *58*(6), 665-678. doi:10.1002/glia.20953
- Rela, L., Piantanida, A. P., Bordey, A., & Greer, C. A. (2015). Voltage-dependent K⁺ currents contribute to heterogeneity of olfactory ensheathing cells. *Glia*, *63*(9), 1646-1659. doi:10.1002/glia.22834
- Richter, M. W., Fletcher, P. A., Liu, J., Tetzlaff, W., & Roskams, A. J. (2005). Lamina propria and olfactory bulb ensheathing cells exhibit differential integration and migration and promote differential axon sprouting in the lesioned spinal cord. *J Neurosci*, *25*(46), 10700-10711. doi:10.1523/JNEUROSCI.3632-05.2005
- Rieger, A., Deitmer, J. W., & Lohr, C. (2007). Axon-glia communication evokes calcium signaling in olfactory ensheathing cells of the developing olfactory bulb. *Glia*, *55*(4), 352-359. doi:10.1002/glia.20460
- Seifert, G., Henneberger, C., & Steinhauser, C. (2018). Diversity of astrocyte potassium channels: An update. *Brain Res Bull*, *136*, 26-36. doi:10.1016/j.brainresbull.2016.12.002
- Stavermann, M., Meuth, P., Doengi, M., Thyssen, A., Deitmer, J. W., & Lohr, C. (2015). Calcium-induced calcium release and gap junctions mediate large-scale calcium waves in olfactory ensheathing cells in situ. *Cell Calcium*, *58*(2), 215-225. doi:10.1016/j.ceca.2015.05.003
- Su, S., Ohno, Y., Lossin, C., Hibino, H., Inanobe, A., & Kurachi, Y. (2007). Inhibition of astroglial inwardly rectifying Kir4.1 channels by a tricyclic antidepressant, nortriptyline. *J Pharmacol Exp Ther*, *320*(2), 573-580. doi:10.1124/jpet.106.112094
- Tang, X., Schmidt, T. M., Perez-Leighton, C. E., & Kofuji, P. (2010). Inwardly rectifying potassium channel Kir4.1 is responsible for the native inward potassium conductance of satellite glial cells in sensory ganglia. *Neuroscience*, *166*(2), 397-407. doi:10.1016/j.neuroscience.2010.01.005

- Whitcroft, K. L., Cuevas, M., Haehner, A., & Hummel, T. (2017). Patterns of olfactory impairment reflect underlying disease etiology. *Laryngoscope*, *127*(2), 291-295. doi:10.1002/lary.26229
- Yao, R., Murtaza, M., Velasquez, J. T., Todorovic, M., Rayfield, A., Ekberg, J., . . . St John, J. (2018). Olfactory Ensheathing Cells for Spinal Cord Injury: Sniffing Out the Issues. *Cell Transplant*, *27*(6), 879-889. doi:10.1177/0963689718779353